Aerodynamic Optimization of Two Element F1 Car Rear Wing

– Assignment 3 2023

Tarun Teja, (tarna588)
Abhishek Dhiman, (abhdh352)

LINKÖPINGS UNIVERSITET

Linköping University
Division of Applied Thermodynamics and Fluid Mechanics
Scientific Report

1 Introduction

Design optimisation is the necessity of the modern world in almost all fields of study. In this study the design optimization is focused on maximizing the aerodynamic performance of motor cars, especially F1 race car with optimization of two element wing (front and rear). There are two vital aerodynamic optimization objectives with primary focus on maximizing the downward force and minimizing axial force (drag) being secondary focus. The main parts generating the aerodynamic downward force in a race car are the front wing, rear wing, and diffuser, [1]. Among these the most influential parts are considered as the front and rear wing. The front wings are the first part to interact with undisturbed air and the generated wake interacts with other parts of the car. The front wings help in producing significant amount of downward force along with streamlining the sweep of air around the car body. The rear wing function is similar to that of front wing with additional benefit of changing the elements (airfoil) angle based on the driving conditions and the track to achieve required downward force, [1] . In the present study, the optimization approach mainly focuses on rear wing of the car which generates large amount of downward force and helps the vehicle to stay on the track at high speed turns. The downward force generation is extremely important while executing sharp turns and overtaking at the turns, hence enhancing the downward force can increase the performance of car's cornering speeds with a penalty of extra drag force. Thus, the two elements wing optimization for a race car for better cornering performance and downward force improvement with small drag penalty is an important field for optimization.

The possible geometric constraints on the two element wing are the size (chord of airfoil), location (relative to each other) and orientation (angle of attack of the airfoils). For the present study, the horizontal and vertical location, and relative orientation of 2nd element w.r.t 1st element are selected. The 2nd element location becomes important to comply with the overall dimensions of the race car and legal tolerance limits. This is done give room for manufacturing discrepancies w.r.t to CAD models of the car during inspection and prevent the possible aerodynamic gain from extra dimensions, [2]. The relative angle change for 2nd element is important to alter the downward force at the required conditions.

The primary objective of the study is the indirect optimization of relative orientation and position of the 2^{nd} element of a two element rear wing to achieve the maximum down force. The secondary focus is on the utilization and comparison of various response surface types for same design of experiment (DoE) and evaluate the discrepancies in the optimized design point. The comparison between various schemes is based on various criteria which are discussed in detail in the following sections. The exploration of optimal design point by means of computational frameworks is faster, more flexible and usually cheaper to simulate a good design space. Hence, one the main reasons for the growing popularity of Computational Fluid Dynamics (CFD) in both industry and academia.

2 Methodology

The Response Surface generation is the basis of the methodology for which the design space is created using Optimal Space Filling (OSF) scheme. The range of each output parameter is explored by the Response Surface Optimization algorithm to obtain the optimized values of input parameters by satisfying the objective functions. The details are explained in subsequent sub-sections.

2.1 Domain size and mesh

This section highlights the mesh requirements, computational domain size, boundary conditions and other details related to the CFD pre-processes of two dimensional study of the two element rear wing. To carry out any CFD simulations it is necessary to define flow region or domain size. The size of the domain size is chosen in such a way that it captures all the essential flow interaction without being very large. A large domain size is associated with longer simulation run times and higher computational costs. After careful considerations, multiple refinement region are created inside the domain to prevent sudden jumps in aspect ratio of mesh element and provide smoother transition to primary region of interest. The middle refinement has size of width 6c (c = chord length of element/airfoil 1) and length 9c. The outer is made up of coarser triangular elements and the domain size 25c X 25c, Fig.1a.

An unstructured mesh (triangular elements) is used which is easier to generate and better refinement can be applied in the region of interest, Fig. 1b. Two bodies of influence are used to generate the mesh and prevent abrupt jumps in element aspect ratio. Edge sizing is employed along with the inflation with 21 on both airfoils resulting in $y^+ < 1$ on both the airfoils. The inner most sphere of influence is scoped to control and keep transition away from airfoils and plays a vital role in capturing the flow physics, Fig.1b

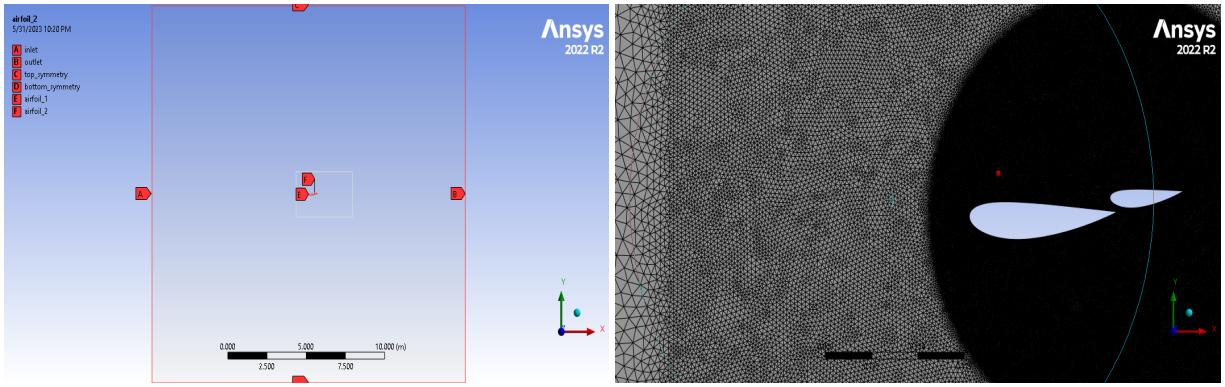

(a) Domain size 20c boundaries **(b) Unstructured mesh & body of influences**

Figure 1: Domain and Mesh with body influences

2.2 Boundary conditions and solver setup

The CFD simulations carried out in the present study are executed in Ansys Fluent (2022 R2) using steady state and k – ω SST turbulence model with low - R_e correction enabled to damp the turbulent viscosity in sub-viscous layer [3]. The model is used to capture the sections of boundary layer and flow separation and reversal effects at higher (α_2) i.e 2nd element orientation. Pressure based solver is used as the flow regime is low subsonic with air as working fluid. The numerical scheme is second order upwind spacial discretization, least squares cell based for gradient and coupled solver for Pressure-velocity coupling. Boundary condition at inlet is set as velocity-inlet with $V_x = 19.445$ [m/s] (70 kmph) i.e slow corner speed for F1 [4]. The symmetry boundary condition is used at the upper and the lower domain boundary as they are sufficiently far from the airfoils to hinder the velocity profile. Both the airfoils had no-slip wall leading to boundary layer formation. The outlet condition is pressure outlet with zero gauge pressure.

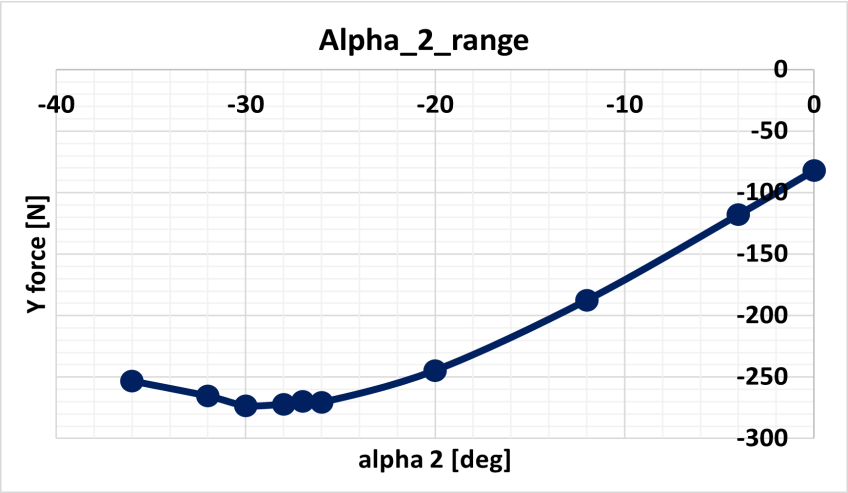

Figure 2: Element 2 orientation (α_2) range for DoE

2.3 Design of Experiment (DoE)

The purpose of Design of Experiment is to gather a representative set of data to compute and generate a response surface model, and then run an optimization. Basically, DoE represents the set of design points that are evaluated systematically and covers the entire design space. The quality of response surface is greatly dependent on DoE scheme which determines the exact simulations to be run to generate a response surface. For a two element rear wing optimization to generate the maximum downward force, the selected input variables are the orientation of 2nd element (α_2), horizontal position (X) from 1st element leading edge (LE) and vertical position (Y) from 1st element trailing edge (TE). These parameters corresponds to optimistic characterization of two element rear wing (airfoil) to create the maximum downward force. The input variables vary in a continuous manner in a specific range. The range is user defined consisting of upper and lower bounds for all the input parameters. The DoE can be created using several schemes, in this study Optimal Space Filling (OSF) and Central Composite Design (CCD) are the primary choices out of which OSF is selected. In essence, OSF is initialized as Latin Hypercube Sampling Design (LHS) and then optimized several times, remaining a valid LHS. The OSF distributes are design points evenly in the design space, aims to achieve high analytical vision with least design points and computationally inexpensive [5]. On the other hand, Central Composite Design (CCD) which divides the input parameter range in five segments $[-\alpha, -1, 0, 1, +\alpha]$ resulting in a quadratic function and required large design points for fewer variables [6].

The Airfoil NACA-4421 was re-utilised from the previous study for both elements of rear wing. The chord length (c) element/airfoil 1 is 400 mm at $\alpha_1 = 1^\circ$ and for airfoil 2c = 200 mm at $\alpha_2 = 4^\circ$ as base configuration.The reference frame of airfoil 2 has trailing edge (TE) of airfoil as the origin i.e (400, 0). The distance between two sections must lie in between 10-15 mm at their closed position, [2]. Hence, five X positions are selection for airfoil 2 leading edge (LE) w.r.t airfoil 1 TE i.e -20(380 mm), -10(390 mm), 0(400), 10(410 mm) and 20(420 mm). Similarly, five locations in positive Y direction at [40, 50, 60, 70, 80] (mm) are selected.

The $\alpha_1 = -1^\circ$ is kept constant and the range for α_2 is restricted to (0 to -30°(inverted)) based on the parametric analysis, Fig. 2. After (-26°) the flow separation at TE was observed to begin leading to drag force increment. Also, above (-30°) the down force is reduces due separation and wake formation.

2.4 Grid Independence Study

Mesh independence study is used to estimate the mesh induced error on the results and use the mesh with error below 5% [7]. The main objective is to find a mesh with sufficiently high accuracy with low computational cost. The grid study was performed for 5 different meshes by checking the results for combined normal and axial force of the airfoils. The mesh details and mesh growth rate (rGR) are presented in Table. 1. Thee results for ForceX_{e1_e2} and ForceY_{e1_e2} for all mesh are plotted in Fig. 3 highlighting the convergence achieve with mesh refinement. The lift and drag are stabilized for mesh3 with %error 1.813% and 2.01% respectively. Hence, mesh3 is selected for all the simulations.

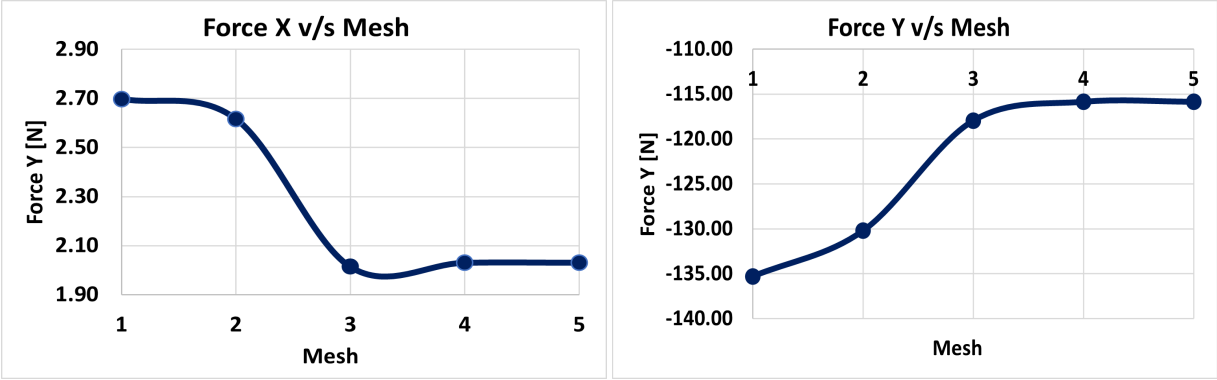

(a) Drag force (ForceX_{e1_e2}) **(b) Lift force** (ForceY_{e1_e2})

Figure 3: Drag force and lift-force convergence for grid independent study

Mesh Independence Study

Mesh	Nodes	Elements	h(value)	r(GR)	ForceX	ForceY	% ErrorX	% ErrorY
M1	50626	82080	69.819		2.698	-135.29	16.7	17.02
M2	111228	218548	42.787	1.632	2.616	-130.2	12.3	12.62
M3	233380	455662	29.633	1.444	2.014	-117.94	1.813	2.01
M4	427172	836998	21.864	1.355	2.031	-115.84	0	0.198
M5	616378	1214244	18.153	1.205	2.031	-115.849	0	0

2.5 Optimization Methodology

In the present study, Indirect optimization is performed which analytically creates the necessary and sufficient conditions for optimality, which are then solved numerically [8]. This statistical i.e Response Surface Methodology (RSM) is part of indirect optimization which uses DoE to obtain and optimal response [9]. In the present study, four response surface types are used for the same problem statement in order to estimate the discrepancies in the optimized input variables and compare the strength and weaknesses for each. once the response surface is generated, next is the optimization process. In this study, there are three input variables $\alpha - 2$, X position and Y position of 2^{nd} element as explained above and three objective functions are specified, hence optimization is performed using Multi Objective Genetic Algorithm (MOGA). The objective functions are to minimize (downforce_airfoil1), minimize (downforce_airfoil2), and minimize (downforce_both_airfoils_combined), here minimize implies the maximum downforce (negative sign).

3 Results

The results obtained for four response surface types [Genetic Aggregation (GA), Full 2^{nd} order Polynomials (2^{nd}) OP, Non-parametric Regression (NPR) and Kriging (KR)] are presented in this section. Each scheme has it's own merits and de-merits, hence optimization is performed using 4 different schemes to estimate the feasible optimized design points with associated trade-off. Design point obtained from each statistical scheme is compared against the simulation to evaluate a % error. The quality of DoE is visualized using various methods like Goodness of Fit curves, Response Surface Charts and sensitivity curves. Further, the post optimization results are presented in form of a table for 3 optimal design points for achieved maximum down force (negative lift). The axial force (drag) did not show significant variation ($\alpha_2 < -30°$) till small flow separation hence the results section is more oriented towards down force estimation.

3.1 Goodness of Fit

The goodness of fit plots are shown in Fig. 4 and signifies the quality of fit between output parameters in the test medium (against verification points) and the values obtained from the production of response surface. In general, the fit is in good agreement for all 4 response surface types. The Goodness of Fit plot for GA Fig.4a and KR Fig.4d show better fit with verification points leading to high approximation accuracy on DoE points. Specially, KR with automatic refinement for improved accuracy has perfect fit compared to GA implying highest stability and reliability. For 2^{nd} OP type Fig.4b the verification points do not fit well with the curve implying lower accuracy and stability of response surface prediction with generated DoE points. Finally, the goodness of Fit for NPR, Fig.4c shows high accuracy discrepancies accounting for low quality of predicting the verification points when compared to all other models. The outlier verification points w.r.t the DoE points makes the NPR least reliable for problem focused in this study.

3.2 Response Surfaces

The response surface facilitate the exploration of design space by graphical means, depicting the effects of two input parameters (X and α_2) on one output parameter (ForceY). Each surface, Fig.5 provides the ability to visually explore the design space and design points from DoE to estimate the influence of input parameters on output parameters. All the response surfaces in Fig. 5 use the same DoE, but estimates the optimal response surface with slight variation, majorly seen for NPR in Fig. 5c.

The blue regions represent the maximum down force (**ForceY**) which gets captured in similar fashion for GA (Fig.5a), 2^{nd} OP (Fig. 5b) and KR (Fig.5d). The three algorithm (GA, 2^{nd} OP and KR) show higher stability and prediction accuracy w.r.t Goodness of Fit compared to NPR. More on the comparative analysis, the 2^{nd} OP and KR are closest in terms of response surface capturing the influence X and α_2 on the ForceY compared to GA. Also the tendency of KR to show fluctuations on the response surface and lack of smoothness is not present for problem statement of present study and show high surface similarity with GA and 2^{nd} OP. On the other hand, NPR (Fig. 5c) tries to fit the maximum amount of design points in the built in tolerance limits leading to narrowing down the blue region significantly. But in attempt of doing so losses the stability with the prediction points and induces inaccuracies as discussed in Section.3.1.

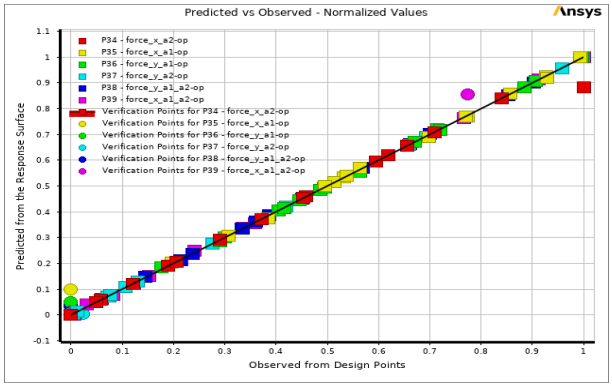

(a) GA goodness fit plot

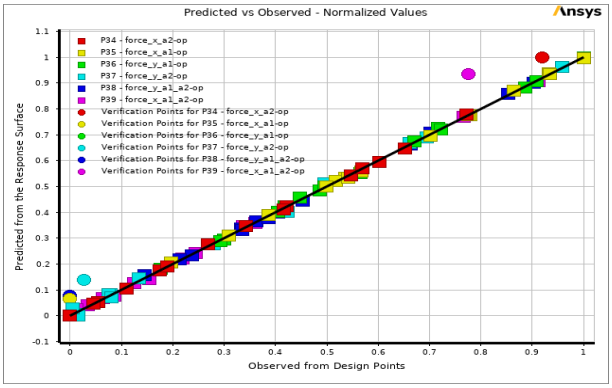

(b) 2nd OP goodness fit plot

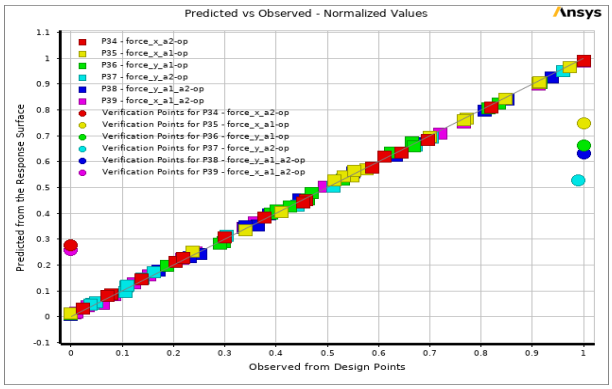

(c) NPR goodness fit plot

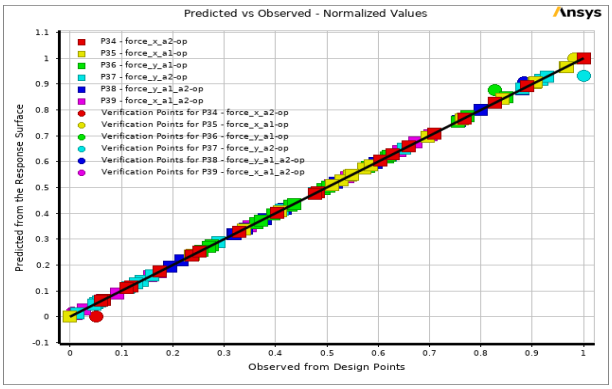

(d) KR goodness fit plot

Figure 4: Goodness of Fit table for all Response Surface types

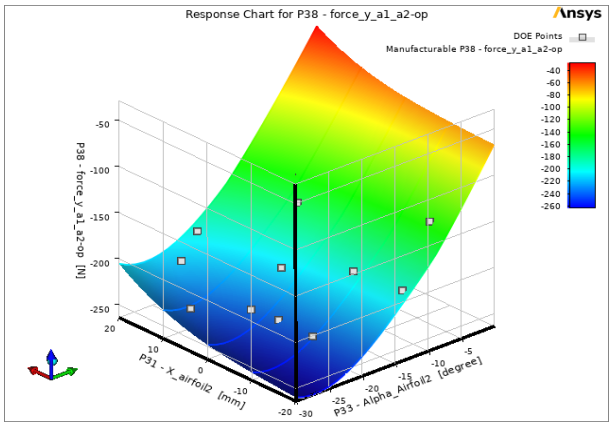

(a) GA response surface

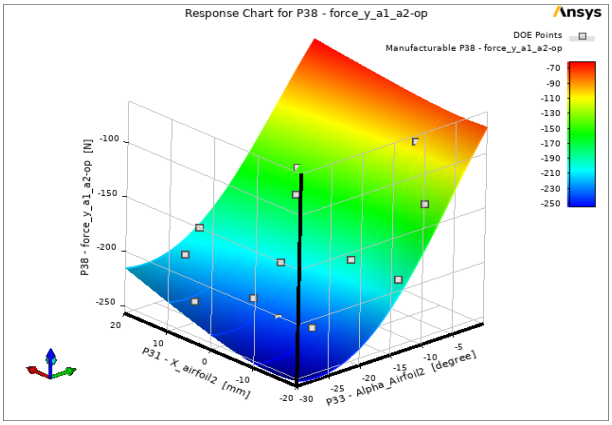

(b) 2nd OP response surface

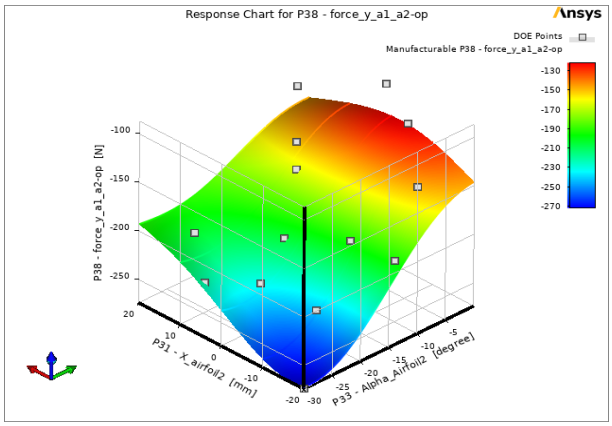

(c) NPR response surface

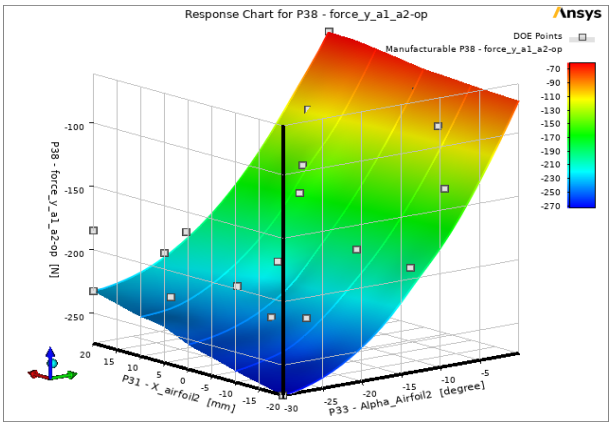

(d) KR response surface

Figure 5: Response surface contours for all Response Surface types

3.3 Local sensitivity Curves

The Local sensitivity curves (Fig. 6) represent the input parameter sensitivity for 1/3 optimized design point (discussed later in report). The output parameter used is the total down force from the two element rear wing and how sensitive it is for each input variable. The response surfaces are visually limited to a few input parameters in capturing the influence. But the local sensitivity curve highlight the sensitivity of the selected output parameter (total down force) for all input parameters. This mean that design exploration calculates the change in each output parameter based on the change in each input parameters independently.

In the local sensitivity curve Fig. 6 the impact of each input parameter on total down force (ForceY) can be seen. The GA (Fig. 6a), 2nd OP (Fig. 6b) and KR (Fig. 6d) show the same sensitivity trends for position (X & Y) and orientation (α_2) variables whereas the NPR (Fig. 6c) under estimates α_2 and Y sensitivity, but over-estimates for X position on the total down force. The mis-match of estimation can be associated with unstable and induced errors by NPR as explained earlier. In holistic view the down force is highly sensitive to the X position and α_2, and least towards the Y position. The sensitivity estimation can also be made visually from the respective curve slope, higher the slope implies higher sensitivity of the input parameter.

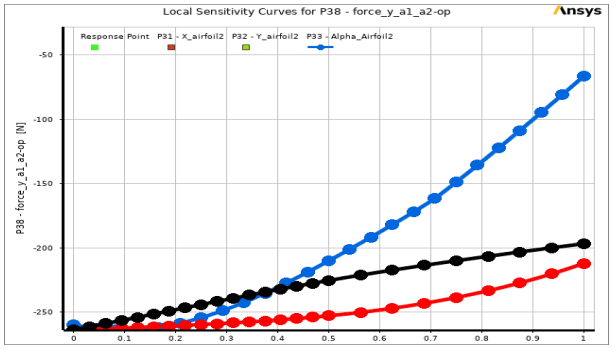

(a) GA Local Sensitivity Curve

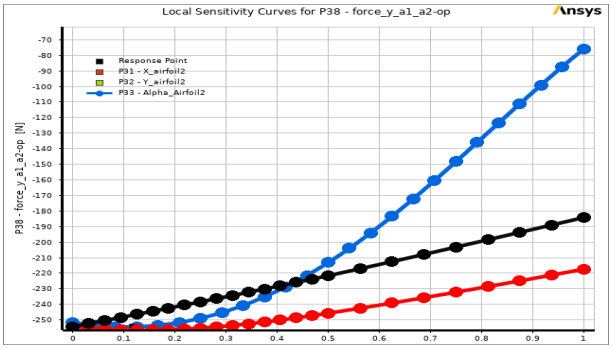

(b) GA Local Sensitivity Curve

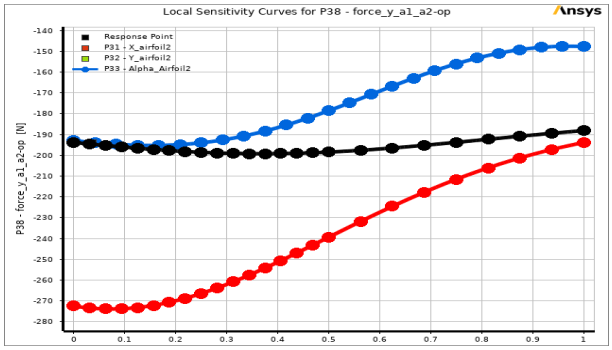

(c) NPR Local Sensitivity Curve

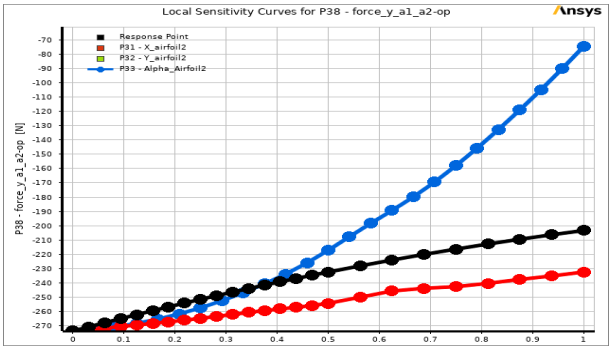

(d) KR Local Sensitivity Curve

Figure 6: Local Sensitivity Curves with α_2(Blue), Y(Black) and X(Red)

3.4 Optimization Results

There two goal-driven optimization systems in Ansys: Response surface optimization and Direct optimization. For this study Response surface optimization system is selected that draws its own response surface cell and is dependent on the quality of the response surface. The obtained results from all 4 response surface types are presented in 7 with three candidate points for each. The maximum downforce estimated is -278.02 (GA candidate3), -275.1 (2nd OP candidate3), -275.56 (NPR candidate1) and -273.76 (KR OP candidate1). The X and Y locations estimated by GA, NPR and KR are same (-20, 40) w.r.t airfoil1$_{TE}$. The 2nd OP differs in X position,

estimating it to be closer to the airfoil1$_{TE}$ for the equal amount to downforce as NPR. The optimizied $\alpha-2$ range [GA (–27.845°), 2nd OP (26.407°), NPR (–28.97°), KR (–29.99°)] relative to $\alpha_1 = -1°$.

The optimized design points obtained using RSM are simulated with the methodology and boundary conditions explained earlier. The results are tabulated in Table. 2 with the % error. The least error is shown by GA and 2nd OP and the highest by NPR. Hence, the optimized design point for maximum downforce is X=-20, Y=40 and $\alpha_2 = -27.845°$ by candidate3 of Genetic Aggregation.

Response_Surface_Type	candidate1				candidate2				candidate3			
Design parameters	X	Y	Alpha2	DownForce (N)	X	Y	Alpha2	DownForce (N)	X	Y	Alpha2	DownForce (N)
Genetic Aggregation	-20	40	-27.923	-275.79	-20	40	-27.884	-276.4	-20	40	-27.845	-278.02
2nd Order Polynomial	-10	40	-26.294	-264.96	-10	40	-26.356	-273.02	-10	40	-26.407	-275.1
Non Parametric Regression	-20	40	-28.97	-275.56	-20	40	-28.914	-275.24	-20	40	-28.853	-275.16
Kriging	-20	40	-29.998	-273.76	-20	40	-29.919	-273.71	-20	40	-29.839	-269.6

Figure 7: Optimized design point comparison for different response surface types

Comparison with CFD results

Response Surface	Candidate	Optimization (N)	CFD (N)	% Error
Genetic Aggregation	candidate3	-278.02	-278.028	0.003
2nd Order Polynomial	candidate3	-275.1	-275.09	0.003
Non Parametric Regression	candidate1	-275.56	-277.02	0.53
Kriging	candidate1	-273.76	-273.63	0.048

4 Discussion

The DoE quality assessment estimated from Goodness of Fit, Fig. 4 for all the response surface types showed KR to be the ideal choice. Also, the response surface 5d and sensitivity analysis 6d obtained for KR is similar to two other schemes i.e. GA and 2nd OP. The discrepancies observed in NPR for goodness of fit Fig. 4c are due to high tolerance consideration of NPR scheme which force it include most of the design points, [10], hence the shape of the response surface showed weak resemblance to other schemes, Fig. 5c. The under-lying high tolerance of NPR also resulted in the highest % error for the maximum down force for an optimized design point 2. Another observation is the variation of optimized X position (-10) obtained from 2nd OP which different from all other schemes i.e (-20). The is due to the quadratic nature of the 2nd OP [10] limiting its flexibility towards the fluctuations in DoE when compared to high tolerance of NPR and auto refinement of KR and GA resulting in highest variation in downforce among its optimized three candidates.

Complementing to the GA, and KR optimization is the coefficient of determination (R = 1) for most of the output variables. Also, the root mean square error and the average absolute error values for all the candidate points are close to 0, highlighting the good quality of response surface. Similarly, the relative maximum absolute error and relative average absolute error of the verification points (Quality of prediction) is very poor at all output parameters. Subsequently, the obtained goodness of fit for GA, Fig. 4a and KR, Fig. 4d showed highest quality for DoE

among the 4. The utilization of learning points for cross validation by GA and inclusion of fluctuations function (local deviations) along with quadratic function in KR are the strengths of the two resulting in an effective way to assess the stability and quality of the DoE [10]. Additional strength of GA and KR is the automatic refinement for increase accuracy and quality of response surface hence making the two algorithm highly reliable for optimized values. The 2^{nd} OP response surface is solely the quadratic function model and the verification points are too far from the best value region in order to maximize the distance to the learning points, Fig. 4b, 5b. Therefore, leading to inaccuracies quality of prediction and in-ability to capture fluctuations in the response surface [10]. Finally, the goodness of fit and local sensitivity estimated by NPR are the odd one out among all but with the in-built dynamic tolerance ability manages to generate optimized parameters similar to GA and KR, Fig. 7.

The optimized input variables obtained from all 4 response surface methods signifies that the 2^{nd} element/airfoil must be at the minimum Y position out of all considered in this study result higher flow acceleration and pressure difference on airfoil2 leading to immense downforce. Secondly, the X position should be such that it hides the airfoil1 trailing edge (TE) in a top view implying it to be between -20 to -10 [mm] of the airfoil1 TE, also mention in the FIA regulations [2]. The over-lapping X position of airfoil2 w.r.t airfoil1 allows flow transition from pressure side of airfoil1 to suction side of airfoil2. Eventually, the α_2 being limited to $-30°$ to prevent flow separation and wake aided in pin pointing the range to $-26° < \alpha_2 < -30°$, Fig. 7. The range for α_2 seems high relative to $\alpha_1 = -1°$, which make the higher angles of this range more susceptible to flow separation. To prevent the same, the lower α_2 as estimated by GA and 2^{nd} OP ($\alpha_2 < 28°$) are more favourable.

Computation wise GA utilized more time than classical response surfaces i.e. 2^{nd} OP, NPR and KR models due to the fact that GA uses multiple solvers and cross validation points hence making it more reliable. Next in queue is Kriging (KR) with higher order functioning to capture fluctuations and auto-refinement aiding in highest quality of response surface and goodness of fit but lacks cross validation capability of GA. The KR model also acts as a meta modeling algorithm which give the improved quality of response surface by considering more points as refinements to design domain and convergence is achieved [10]. But due to refinement points the predicted relative error becomes large for present output parameters which is a possible reason for significant gap of 4.26 [N] in the optimized value downforce comparative to GA. Finally, the remaining response surface models 2^{nd} OP and NPR showed trade-off between the response surface accuracy and computational time, these current settings help in producing good results however some deviations are observed for local sensitivity and response surface.

5 Conclusions

The presented study focused on 2D analysis and optimization of multi-element wing (F1 rear wing) are summarized as follows.

- The indirect optimization methodology i.e. (RSM) showed great agreement with CFD simulation.
- The comparison of 4 response surface (RS) types for same DoE resulted in % error $< 1\%$ compared to CFD results.
- The quality of DoE estimated by NPR showed great discrepancies and 0.53% error compared to CFD which is highest among the 4 which could significantly increase with increment in design space.

- The 2nd OP with quadratic nature, lacking the high tolerance and auto refinement for improved accuracy is computationally in-expensive and showed lowest % error along with GA i.e 0.003% compared to CFD.
- For the fixed $\alpha_1 = -1°$, the relative α_2 range to prevent downforce reduction due to flow separation is [0° to –30°]
- The optimized input parameters Y for achieve maximum downforce keeps the airfoil2 closest (40 mm) to airfoil1 based on the data selected for this study.
- The X position of airfoils (LE) is -20 mm to -10 mm from airfoil1 TE having chord of 400 mm.
- The α_2 should be in range [–26° to –28°] relative to α_1 at optimized X and Y positions to generate maximum downforce.
- The most appropriate optimized set of input parameters for airfoil2 LE coordinates and AoA is [-380 mm, 40 mm, –27.845°] generated by Genetic Aggregation method.
- The 2nd Order Polynomial and Non Parametric Regression models are computational in-expensive and generated fairly good results compared to Genetic aggregation and Kriging.

References

[1] This is Downforce in F1 (Formula 1) â Easy explained;. Available from: https://formulapedia.com/downforce-in-f1/.

[2] Rear Wing configuration;. Available from: https://www.fia.com/sites/default/files/formula_1_-_technical_regulations_-_2022_-_iss_9_-_2022-02-18.pdf.

[3] Standard k- ω Model;. Available from: https://www.afs.enea.it/project/neptunius/docs/fluent/html/th/node66.htm.

[4] HOW FAST DO F1 CARS GO AROUND CORNERS?;. Available from: https://onestopracing.com/how-fast-do-f1-cars-go-around-corners/.

[5] DOE Other Models;. Available from: https://www.mr-cfd.com/doe-other-models/.

[6] ANSYS DOE and Design Optimization Tutorial;. Available from: https://designinformaticslab.github.io/productdesign_tutorial/2016/11/20/ansys.html#doe.

[7] Fred Stern HWC Robert V Wilson, Paterson EG. VERIFICATION AND VALIDATION OF CFD SIMULATIONS. 1999.

[8] Trajectory optimization;. Available from: https://en.wikipedia.org/wiki/Trajectory_optimization.

[9] Response surface methodology;. Available from: https://en.wikipedia.org/wiki/Response_surface_methodology.

[10] Response Surface Methodology (RSM) Types;. Available from: https://www.mr-cfd.com/response-surface-methodology-rsm-types/.